Available online at www.sciencedirect.com
SCIENCE DIRECT
Journal of Loss Prevention in the Process Industries 18 (2005) 152–166
Journal of Loss Prevention in the process industries
www.elsevier.com/locate/jlp

Laminar burning velocities of hydrogen–air mixtures from closed vessel gas explosions

A.E. Dahoe*

Faculty of Engineering, University of Ulster, FireSERT (Block 27), Co. Antrim, Shore Road, Newtownabbey BT37 0QB, Northern Ireland, UK

Received 31 January 2005; received in revised form 24 March 2005; accepted 29 March 2005

Abstract

The laminar burning velocity of hydrogen–air mixtures was determined from pressure variations in a windowless explosion vessel. Initially, quiescent hydrogen–air mixtures of an equivalence ratio of 0.5–3.0 were ignited to deflagration in a 169 ml cylindrical vessel at initial conditions of 1 bar and 293 K. The behavior of the pressure was measured as a function of time and this information was subsequently exploited by fitting an integral balance model to it. The resulting laminar burning velocities are seen to fall within the band of experimental data reported by previous researchers and to be close to values computed with a detailed kinetics model. With mixtures of an equivalence ratio larger than 0.75, it was observed that more advanced methods that take flame stretch effects into account have no significant advantage over the methodology followed in the present work. At an equivalence ratio of less than 0.75, the laminar burning velocity obtained by the latter was found to be higher than that produced by the former, but at the same time close enough to the unstretched laminar burning velocity to be considered as an acceptable conservative estimate for purposes related to fire and explosion safety. It was furthermore observed that the experimental pressure–time curves of deflagrating hydrogen–air mixtures contained pressure oscillations of a magnitude in the order of 0.25 bar. This phenomenon is explained by considering the velocity of the burnt mixture induced by the expansion of combusting fluid layers adjacent to the wall.

Keywords: Explosion; Burning velocity; Hydrogen

1. Introduction

The present paper describes the determination of the laminar burning velocity of hydrogen–air mixtures from closed vessel gas explosions. Available methods to determine the laminar burning velocity rely on measurements of the flow structure of stabilized flames, the observation of moving flames in the course of confined deflagrations in an optically accessible explosion vessel, or the measurement of pressure variations caused by confined deflagrations in a windowless explosion chamber. The last method, which is the one adopted in the present work and called the traditional approach (Tse, Zhu, & Law, 2000), allows experimentation at initial conditions of very high pressure and temperature. It was demonstrated by various authors that laminar burning velocities of air mixed with hydrogen (Iijima & Takeno, 1986; Milton & Keck, 1984), methane (Agnew & Graiff, 1961; Iijima & Takeno, 1986), propane (Agnew & Graiff, 1961; Babkin, Bukharov, & Molkov, 1989; Metghalchi & Keck, 1980), *n*-butane (Clarke, Stone, & Beckwith, 2001), iso-butane (Clarke et al., 2001), 2-methyl-pentane (Halstead, Pyle, & Quinn, 1974), *n*-heptane (Babkin, Vyun, & Kozachenko, 1967), iso-octane (Babkin et al., 1967; Metghalchi & Keck, 1982), ethylene (Agnew & Graiff, 1961; Halstead et al., 1974), acetylene (Agnew & Graiff, 1961; Rallis, Garforth, & Steinz, 1965), benzene (Babkin et al., 1967), toluene (Agnew & Graiff, 1961; Halstead et al., 1974), indolene (Metghalchi & Keck, 1982), methanol (Metghalchi & Keck, 1982), and acetone (Molkov & Nekrasov, 1981), could be determined by this method. In some cases, the initial conditions were varied up to 50 bar and 700 K.

Because of the growing interest in the use of hydrogen as an energy carrier, it seemed worthwhile to investigate whether the same approach could also be applied to hydrogen–air mixtures. A particular concern was that

* Tel.: +44 28 9036 6073; fax: +44 28 9036 8700.
E-mail address: ae.dahoe@ulster.ac.uk

0950-4230/$ - see front matter © 2005 Elsevier Ltd. All rights reserved.
doi:10.1016/j.jlp.2005.03.007

Nomenclature

Latin symbols

K_G	gas explosion severity index bar (m s^{-1})
m_u	mass of unburnt mixture (kg)
$\boldsymbol{n}$	unit normal (m)
n_0	moles of gas present before explosion (mol)
n_e	moles of gas present after explosion (mol)
P	macroscopic pressure (Pa)
P_0	initial pressure (Pa), reference pressure (Pa)
P_{max}	maximum explosion pressure (Pa)
r_f	flame radius (m)
R	specific gas constant (J kg^{-1} K^{-1})
S_{uL}	laminar burning velocity (m s^{-1})
S^o_{uL}	laminar burning velocity at reference conditions (m s^{-1})
S^*_{uL}	unstretched laminar burning velocity (m s^{-1})
t	time (s)
T	temperature (K)
T_0	reference temperature (K)
T_u	temperature of the unburnt mixture (K)
T_{u0}	initial temperature of the unburnt mixture (K)
$\boldsymbol{v}$	velocity vector (m s^{-1})
V_v	volume explosion vessel (m^3)

Greek symbols

γ	specific heat ratio (–)
ν'_i	stoichiometric coefficient of the ith species on the reactant side (–)
ν''_i	stoichiometric coefficient of the ith species on the product side (–)
ρ	density (kg m^{-3})
ρ_b	density of the burnt mixture (kg m^{-3})
ρ_u	density of the unburnt mixture (kg m^{-3})
ϕ	equivalence ratio (–)

Other symbols

$(dP/dt)_{max}$	maximum rate of pressure rise (Pa s^{-1})
$\mathcal{L}_c$	curvature Markstein length (m)
$\mathcal{L}_s$	stretch Markstein length (m)
$\mathcal{R}$	radius of curvature (m)

the tendency of laminar hydrogen–air flames to develop into wrinkled structures (Aung, Hassan, & Faeth, 1997; Aung, Hassan, & Faeth, 1998; Tse et al., 2000) might render this methodology useless for the experimental determination of the laminar burning velocity. This concern stems from the fact that the use of windowless explosion vessels appears to be unacceptable to some researchers (Tse et al., 2000) because influences of stretch intensity and flame shape, which are inherently coupled to the development of flames into wrinkled structures, are not taken into account. Measurements of the laminar burning velocity that do not take contemporary insights in stretch and curvature effects into account are even considered to be flawed by other researchers (Dowdy, Smith, Taylor, & Williams, 1990). Wu and Law (1984) were the first who measured stretch-free laminar burning velocities by introducing a methodology to subtract stretch effects out from experimental laminar burning velocities of flames in stagnation flows. This work inspired the subsequent use of counter-flow flames for the determination of stretch-free laminar burning velocities (Law, Zhu, & Yu, 1988; Yu, Law, & Wu, 1986; Zhu, Egolfopoulos, Cho, & Law, 1989; Zhu, Egolfopoulos, & Law, 1989) and attempts to compensate stretch effects on spherically propagating flames in optically accessible explosion vessels (Aung et al., 1997, 1998; Brown, McLean, Smith, & Taylor, 1996; Dowdy et al., 1990; Hassan, Aung, & Faeth, 1997; Hassan, Aung, & Faeth, 1998; Kwon, Tseng, & Faeth, 1992; Tse et al., 2000; Tseng, Ismail, & Faeth, 1993). However, when stretched and unstretched laminar burning velocities are plotted together (see the upper part of Fig. 5), it is seen that laminar burning velocities of fuel-rich mixtures obtained from a windowless vessel (e.g. the data of Iijima & Takeno, 1986) fall within the scatter of the data obtained by more advanced methods that take stretch effects into account. It is also seen that laminar burning velocities of fuel-lean mixtures obtained from a windowless vessel are consistently larger than stretch-free data. With this being the case, laminar burning velocities from windowless explosion vessels are to be considered valuable for the assessment of accidental combustion hazards, even when they are unacceptable or flawed in the light of more advanced methods. Conversely, if the laminar burning velocities of fuel-lean mixtures had been consistently lower that the stretch-free values, their use as a quick estimate for the assessment of accidental combustion hazards would have been unacceptable.

With the foregoing in mind, it was decided to apply the methodology by Dahoe and de Goey (2003) and Dahoe, Zevenbergen, Lemkowitz, and Scarlett (1996) to the pressure–time curves of hydrogen–air explosions in a closed vessel. It was demonstrated earlier by Dahoe et al. (1996) that this methodology could be applied to turbulent dust explosions in closed vessels to find an estimate of the turbulent burning velocity of a dust–air mixture. In a later contribution, Dahoe and de Goey (2003) demonstrated that it could also be applied to closed vessel gas explosions to find an estimate of the laminar burning velocity of methane–air mixtures. Although it is shown further in this paper that the laminar burning velocities of hydrogen–air mixtures obtained by this approach fall within the scatter of data produced by more advanced methods, it is emphasized that this method should only be applied when the application of more advanced ones becomes impractical.

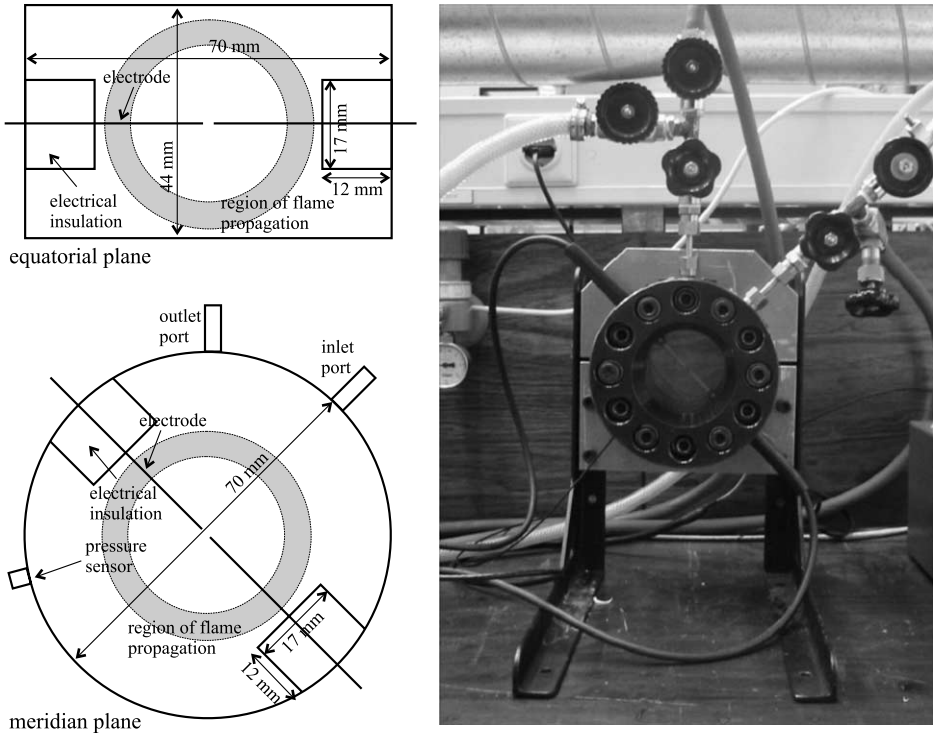

Fig. 1. The experimental setup. Upper-left part: a schematic overview in the equatorial plane. Lower-left part: a schematic overview in the meridian plane. Right part: a photograph of the explosion vessel. The shaded region in the upper-left and lower-left parts indicates the trajectory of the flame that corresponds with the pressure data shown in middle-left and lower-left part of Fig. 6. The latter are used to determine the laminar burning velocity.

2. Explosion behavior of hydrogen–air mixtures in a 169 ml vessel

A cylindrical explosion vessel with a diameter of 70 mm and a length of 44 mm, and hence, a volume of 169 ml, was used in the present work. The reason for choosing such a small volume was to achieve a significant amount of pressure buildup before buoyancy effects would manifest themselves, as discussed by Dahoe and de Goey (2003). A photograph of the explosion vessel is shown in the right part of Fig. 1. Its dimensions on an equatorial and a meridian intersecting plane are given in the left part of the same figure. The vessel is constructed from stainless steel, with quartz windows mounted on its end caps. The cylinder mantle houses a piezo-electric pressure sensor, an inlet port to admit gases, and an outlet port to dispose combustion products. Tungsten electrodes with a diameter of 1 mm, entering through the cylinder mantle, were used to enable spark ignition within a gap of 2 mm at the center of the vessel. The sparks used in the present work had a duration of less than 25 μs and an energy of about 100 mJ. To prevent spark discharges from the electrodes to the vessel wall, the electrical insulation of a diameter of 17 mm, was extended into the interior of the vessel over a length of 12 mm, thereby reducing the effective volume to 165 ml.

A series of experiments was conducted with initially quiescent hydrogen–air mixtures at an initial pressure of 1 bar and an initial temperature of 293.15 K. Hydrogen–air mixtures of an equivalence ratio of 0.5, 0.75, 1.0, 1.25, 1.5, 2.0, and 3.0 were ignited to deflagration at the center of the vessel, and the behavior of the pressure was measured at a sample-rate of 64 kHz. The pressure–time curves are shown in Fig. 2. Each curve exhibits a similar behavior: after ignition, the pressure in the explosion vessel increases progressively until the rate of pressure rise achieves a maximum, $(\mathrm{d}P/\mathrm{d}t)_{\max}$, and continues to increase with a progressively decreasing rate of pressure rise towards a maximum, $P_{\max}$. Once $P_{\max}$ is reached, the pressure in the vessel begins to decrease. In this respect, the behavior of these pressure–time curves is similar to that of methane–air mixtures in a 20-l explosion sphere (see Fig. 6 of

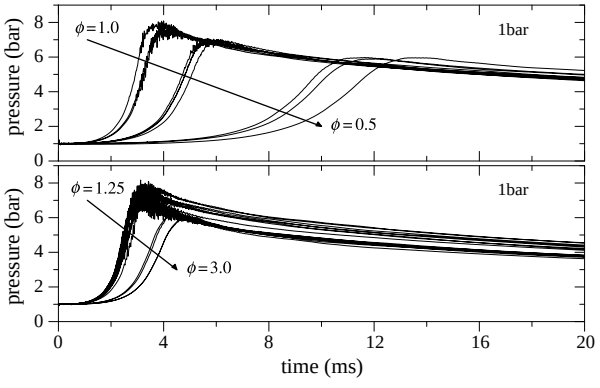

Fig. 2. Measured explosion pressure curves of stoichiometric and fuel-lean hydrogen–air mixtures (top), and fuel-rich hydrogen–air mixtures (bottom).

Dahoe & de Goey, 2003). Despite this similarity the inflection point occurs for a different reason in the 169 ml vessel used in the present work. As discussed previously by Dahoe and de Goey (2003), the duration of an explosion in a 20-l sphere is long enough to allow the flame ball to rise in the vessel due to buoyancy. As a result, there is still a layer of unburnt mixture present below the lower hemispherical part of the flame, after all reactants ahead of the upper hemispherical part of the flame have been consumed. Because the surface area of the lower hemispherical part of the flame decreases progressively during the consumption of the remaining part of the reactants in the final stage of the explosion, the accompanying rate of pressure rise also decreases progressively. Although the role of buoyancy is negligible in the 169 ml vessel, there is still the effect of a progressively decreasing flame surface area in the final stage of the explosion. Initially, the flame ball grows with a progressively increasing flame surface area, until it reaches the wall of the vessel. From that moment onwards, the flame surface area, and hence the rate of pressure rise, decreases progressively as the reactants in the corners of the vessel are being consumed.

It may also be observed from Fig. 2 that, unlike with methane–air mixtures, the pressure–time curves of hydrogen–air mixtures exhibit oscillations whose magnitude may vary up to about 0.25 bar. These oscillations arise with both fuel-lean and fuel-rich mixtures, and tend to become zero when the mixture strength approaches the flammability limits. Their onset occurs before the maximum explosion pressure is reached, after an initial period of smooth pressure buildup, and their presence continues after the explosion has completed. The cause of this phenomenon is described by Garforth and Rallis (1976) and Lewis and von Elbe (1961), Chapter 15, and will be discussed in Section 3.

To enable a comparison with results presented by other researchers, the maximum explosion pressure, P_{max}, and the maximum rate of pressure rise, $(dP/dt)_{max}$, were determined as illustrated by the upper part of Fig. 3. Since the experimental

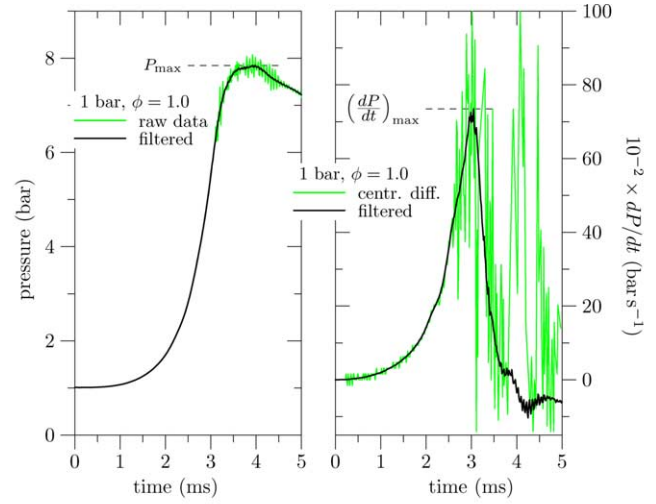

Theoretical maximum explosion pressure

ϕ	0.5	0.75	1.0	1.25	1.5	2.0	3.0
P_{max} (bar)	6.096	7.366	8.011	8.016	7.807	7.35	6.546

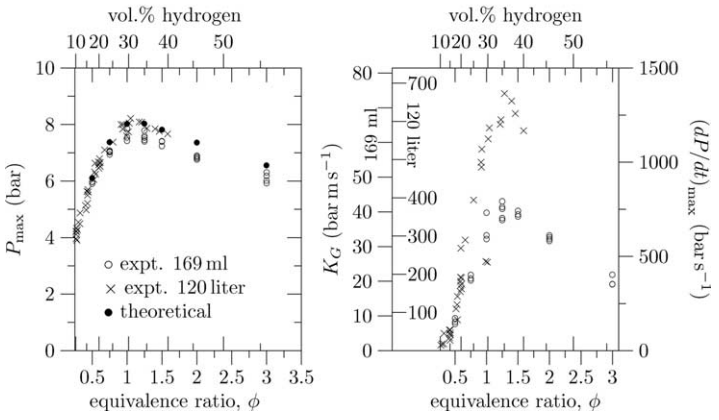

Fig. 3. An illustration of the determination of the maximum explosion pressure, P_{max}, and the maximum rate of pressure rise, (dP/dt), from the measured explosion curve (top), theoretical values of the maximum explosion pressure (middle), and the behavior of the maximum explosion pressure and the maximum rate of pressure rise as a function of the equivalence ratio (bottom).

pressure–time curve contained pressure oscillations, the mean underlying curve and its derivative had to be determined by a smoothing filter. This was accomplished by means of the Savitzky–Golay method (Savitzky & Golay, 1964), using the algorithm `savgol` by Press, Teukolsky, Vetterling, and Flannery (1992) with a second degree polynomial and a data window involving 21 points, namely, 10 on the left, and 10 on the right of the point where the mean value and its first derivative are to be evaluated. The dark curve in the upper-left part of Fig. 3 denotes the filtered pressure–time curve, and the filtered derivative is denoted by the dark curve in the upper-right part. The upper-right part of Fig. 3 also shows the behavior of the time-derivative as obtained from central differencing. It is seen that the points are so heavily scattered around the mean underlying value that the determination of $(dP/dt)_{max}$ becomes meaningless without the application of a smoothing filter.

The lower part of Fig. 3 shows a comparison between the values of P_{max} and $(dP/dt)_{max}$ obtained with the 169 ml vessel, and those measured in a 120 l vessel by Cashdollar, Zlochower, Green, Thomas, and Hertzberg (2000). Theoretical[1] estimates of P_{max}, whose numerical values are tabulated in the middle of the figure, are also plotted in the lower-left part of Fig. 3. A comparison between the maximum explosion pressures shows that practically no difference exists between the values measured by Cashdollar et al. (2000) and the theoretical values. At the same time it may be observed that the maximum explosion pressure in the 169 ml vessel may be up to 10% lower than the theoretical values. This discrepancy may be attributed, to the larger surface to volume ratio, and the consequential larger heat losses in the final stage of the explosion. The lower-right part of Fig. 3 indicates that the maximum rate of pressure rise increases by a factor of about 1.4 when the effective volume of the explosion vessel increases by a factor of about 700. The scales on the left axis of the figure indicate that no formal cube-root-law[2] agreement exists between the maximum rates of pressure rise in the two vessels. The existence of a cube-root-law agreement between the maximum rates of pressure rise in both vessels would cause the scales on the left axis to be identical.

[1] These calculations were performed with GASEQ for the reaction given in footnote 3. GASEQ is a program for computation of chemical equilibria for perfect gasses, written by Chris Morley.

[2] The K_G-value, also known as the gas explosion severity index, is a quantity which forms the design basis of a great deal of practical safety measures. It is defined as the product of the maximum rate of pressure rise and the cube-root of the volume of the explosion vessel, $K_G = (dP/dt)_{max} V^{1/3}$, and believed to be a mixture specific explosion severity index. The K_G-value was defined in this way because it was believed that maximum rates of pressure rise measured in differently sized vessels would become volume-invariant when multiplied by the cube-root of the volume. The practical significance of this quantity rests on the assumption that once it is known for a particular mixture from an experiment in a small laboratory test vessel, the maximum rate of pressure rise in a larger industrial vessel is predicted correctly by dividing it by the cube-root of the larger volume.

3. Oscillations in the pressure–time curve of hydrogen–air deflagrations

Prior to addressing the mechanism behind the pressure oscillations, it is helpful to consider the behavior of the gas contained within a small volume, located around the center of the vessel. At the moment of ignition, the gas contained within this volume burns at constant pressure, which is equal to the initial pressure. After an initial period of expansion, the gas is subsequently compressed to nearly the initial volume it occupied before ignition occurred. The size of a fluid pocket, as well as the temperature of the burnt gases contained within it during the successive stages of expansion and compression may be estimated by means of the adiabatic compression laws:

$$\left(\frac{\rho}{\rho_0}\right) = \left(\frac{P}{P_0}\right)^{-(1/\gamma)}, \quad \left(\frac{\rho}{\rho_0}\right) = \left(\frac{T}{T_0}\right)^{-(1/\gamma-1)}, \quad \text{and} \quad \left(\frac{T}{T_0}\right) = \left(\frac{P}{P_0}\right)^{(\gamma-1)/\gamma}. \tag{1}$$

For a stoichiometric hydrogen–air mixture for example, knowing[3] that the constant pressure and constant volume adiabatic flame temperature are 2386 and 2766 K, and that the maximum explosion pressure after constant volume combustion equals 8.011 bar, the third expression in (1) reveals that the temperature of a fluid pocket at the center rises from 2386 to 4324 K in the course of the explosion. This is more than 1500 K above the constant volume adiabatic flame temperature. At the same time, a fluid pocket of a radius of 1 mm, located at the center of the vessel and containing reactants only, initially expands to spherical region of a radius of 5.7 mm containing only combustion products, and is subsequently compressed to a radius of 1.3 mm. Thus, a fluid particle residing at the boundary of the spherical region undergoes an oscillatory motion: first it moves 4.7 mm away from the center of the vessel, and then it travels 4.4 mm back towards the center.

[3] These flame temperatures and maximum explosion pressure were calculated with GASEQ. The initial temperature was 293.15 K and the chemical reaction

$$\nu'_{H_2}H_2 + \nu'_{O_2}O_2 + \nu'_{N_2}N_2 \rightarrow \nu''_{H_2O}H_2O + \nu''_{O_2}O_2 + \nu''_{N_2}N_2 + \nu''_{H_2}H_2 + \nu''_{HO\cdot}HO^{\cdot} + \nu''_{H\cdot}H^{\cdot} + \nu''_{O\cdot}O^{\cdot},$$

with $\nu'_{H_2} = 0.42$, $\nu'_{O_2} = 0.21$, and $\nu'_{N_2} = 0.79$ for the reactants. The stoichiometric coefficients of the product mixture after combustion at constant pressure were calculated to be $\nu''_{H_2O} = 0.39668$, $\nu''_{O_2} = 0.00679$, $\nu''_{N_2} = 0.79$, $\nu''_{H_2} = 0.01772$, $\nu''_{HO\cdot} = 0.009$, $\nu''_{H\cdot} = 0.00218$, $\nu''_{O\cdot} = 7.227 \times 10^{-4}$, and after constant volume combustion, $\nu''_{H_2O} = 0.3806$, $\nu''_{O_2} = 0.00997$, $\nu''_{N_2} = 0.79$, $\nu''_{H_2} = 0.02824$, $\nu''_{HO\cdot} = 0.01764$, $\nu''_{H\cdot} = 0.0047$, $\nu''_{O\cdot} = 0.00182$. The total number of moles before and after the reaction, n_0 and n_e, is not being conserved: the ratio n_e/n_0 is 0.861.

Similarly, a fluid pocket of a radius of 3 mm, containing only reactants, expands to a spherical region of a radius of 17.1 mm consisting of combustion products only, and is subsequently compressed to a radius of 3.9 mm. Moreover, according to the third expression in (1), a temperature gradient that establishes itself within the burnt mixture, such that the temperature is the highest at the point where ignition occurred, and the lowest at the flame surface. The role of this oscillatory motion as the cause of the pressure oscillations may be assessed by considering what happens to a fluid particle residing between the boundary that separates the burnt mixture from the unburnt mixture, $r_b(t)$, and the vessel wall, R_v (see the upper-left part of Fig. 4).

Initially, the fluid particle is being pushed away from the center by the expansion flow. This process continues until it has been consumed by the flame. Next, the fluid particle continues to move away from the center while being part of the expansion flow until its motion is reversed by the expansion of combusting layers closer to the vessel wall. To facilitate the derivation of an expression for its velocity, the shape of the vessel is idealized to a sphere (with an effective volume of 165 ml, its radius, R_v, becomes 34 mm) and the boundary separating the burnt and unburnt mixture, $r_b(t)$, is viewed upon as if it is an impermeable wall that expands like soap bubble from the center towards the wall with a velocity $\dot{r}_b(t)$. When the location of a fluid particle residing on an arbitrary spherical surface between $r_b(t)$ and the vessel wall is denoted by $r(t)$ (see the upper-left part of Fig. 4), it becomes evident that the ratio of the mass contained between $r_b(t)$ and $r(t)$, and the mass contained between $r_b(t)$ and the vessel wall

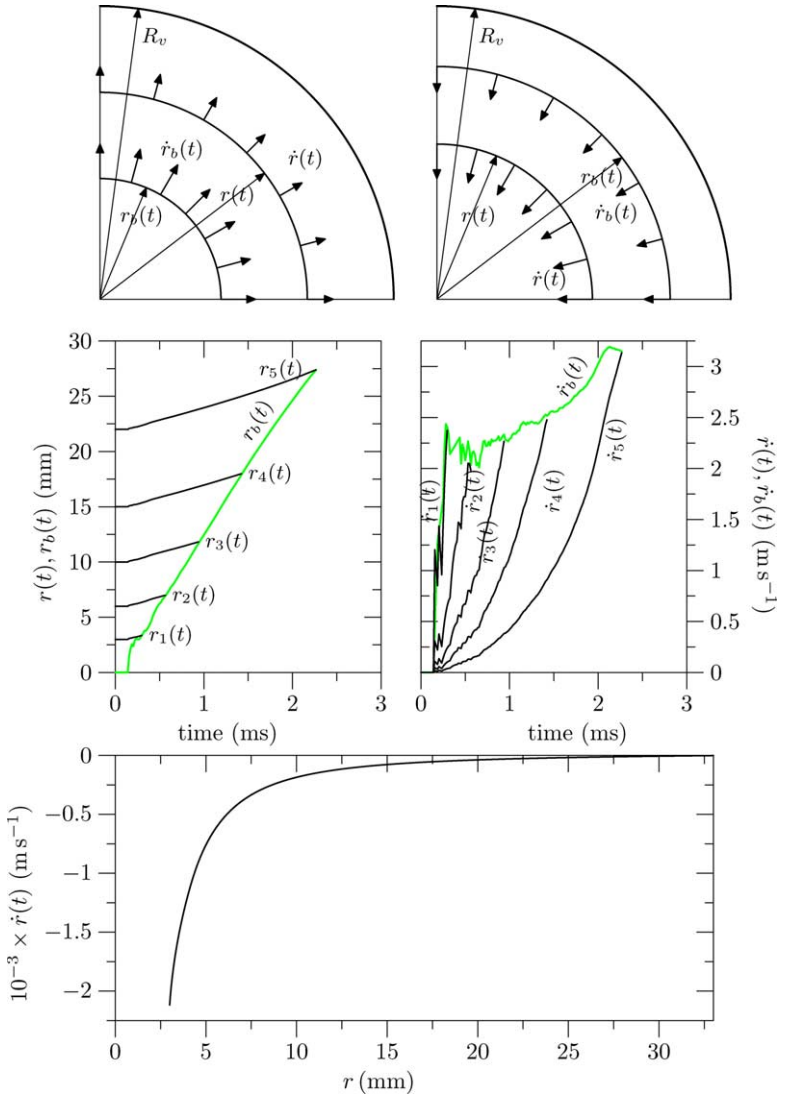

Fig. 4. Effect of compression on the position and velocity of fluid elements. The upper-left part illustrates the compression of the unburnt mixture ahead of an expanding flame. The upper-right part illustrates the compression of the burnt mixture caused by the expansion of combusting layers close to the wall. The middle part shows the behavior of five fluid particles in the unburnt mixture at initial positions, $r_1(0) = 3$ mm, $r_2(0) = 6$ mm, $r_3(0) = 10$ mm, $r_4(0) = 15$ mm, and $r_5(0) = 20$ mm from the center. The lower part shows the behavior of the velocity of fluid particles within the burnt mixture when they are being compressed by an expanding layer close to the wall.

remains constant:

$$\frac{\frac{4}{3}\pi\rho_u[r^3(t)-r_b^3(t)]}{\frac{4}{3}\pi\rho_u[R_v^3-r_b^3(t)]}=\text{constant}. \tag{2}$$

When this expression is differentiated with respect to time

$$\frac{[R_v^3-r_b^3(t)][r^3(t)-r_b^3(t)]'-[r^3(t)-r_b^3(t)][R_v^3-r_b^3(t)]'}{[R_v^3-r_b^3(t)]^2}=0, \tag{3}$$

only the nominator needs to be evaluated

$$[R_v^3-r_b^3(t)][3r^2(t)\dot{r}(t)-3r_b^2(t)\dot{r}_b(t)] + [r^3(t)-r_b^3(t)][3r_b^2(t)\dot{r}_b(t)]=0 \tag{4}$$

$$\Leftrightarrow R_v^3r^2(t)\dot{r}(t)-R_v^3r_b^2(t)\dot{r}_b(t)-r_b^3(t)r^2(t)\dot{r}(t) + r^3(t)r_b^2(t)\dot{r}_b(t)=0 \tag{5}$$

$$\Leftrightarrow r^2(t)[R_v^3-r_b^3(t)]\dot{r}(t)=r_b^2(t)[R_v^3-r^3(t)]\dot{r}_b(t), \tag{6}$$

to obtain the following expression for the velocity of the fluid particle, $\dot{r}(t)$:

$$\dot{r}(t)=\frac{r_b^2(t)}{r^2(t)}\frac{R_v^3-r^3(t)}{R_v^3-r_b^3(t)}\dot{r}_b(t). \tag{7}$$

Since $r_b(t)\le r(t)\le R_v$, it is evident that the velocity of the fluid particle, $r(t)$, cannot exceed $\dot{r}_b(t)$. It is furthermore seen that the fluid particle attains a maximum speed, equal to $\dot{r}_b(t)$ (i.e. the flame speed minus the burning velocity), at the moment when it is being consumed by the flame. Its subsequent motion as a constituent of the burnt mixture is continued with a velocity smaller than $\dot{r}_b(t)$.

The behavior of $r(t)$ and $\dot{r}(t)$ of five fluid particles, initially at a distance of $r_1(0)=3$ mm, $r_2(0)=6$ mm, $r_3(0)=10$ mm, $r_4(0)=15$ mm, and $r_5(0)=20$ mm from the center, along with the behavior of $r_b(t)$ and $\dot{r}_b(t)$, are shown in the middle-part of Fig. 4. The position and velocity of each particle were computed from Eq. (7) and

$$r(t^{n+1})=r(t^n)+\dot{r}(t^n)\Delta t, \tag{8}$$

where $r(t^{n+1})$ denotes the position at a next time, $r(t^n)$ the position at a previous time, and Δt the time increment between two consecutive times. The values of r_b and $\dot{r}_b$, as needed by Eq. (7) were obtained from the filtered pressure–time curve and filtered (dP/dt)-curve shown in Fig. 3 by means of

$$r_b=\left(\frac{3V_v}{4\pi}\right)^{1/3}\left[1-\left(\frac{P_0}{P}\right)^{1/\gamma}\frac{P_{max}-P}{P_{max}-P_0}\right]^{1/3}, \tag{9}$$

which is identical to Eq. (18) for the position of the flame, and its derivative with respect to time

$$\dot{r}_b=\frac{d\dot{r}_b}{dt}=\frac{\partial\dot{r}_b}{\partial P}\frac{dP}{dt} \tag{10}$$

$$\dot{r}_b=\frac{1}{3(P_{max}-P_0)}\left(\frac{3V_v}{4\pi}\right)^{1/3}\left[1-\left(\frac{P_0}{P}\right)^{1/\gamma}\frac{P_{max}-P}{P_{max}-P_0}\right]^{-(2/3)} \times\left[1+\frac{1}{\gamma P}\right]\left(\frac{P_0}{P}\right)^{1/\gamma}\frac{dP}{dt}. \tag{11}$$

The time increment in Eq. (8) was equal to the reciprocal value of the sample-rate (64 kHz) used to measure the experimental pressure curve. If these fluid particles would suddenly lose their motion to become static, the result would be a pressure disturbance of a magnitude of at most $(1/2)\rho_u\dot{r}_b^2(t)$. However, with an assumed value of 1 kg m^{-3} for ρ_u, and the velocities shown in the right-middle part of Fig. 4 the resulting pressure oscillations are negligible. This situation becomes different when particle velocities are induced by the combustion of fluid layers closer to the wall.

Combusting fluid layers closer to wall induce a displacement velocity in the burnt mixture, directed towards the center. This reversal of the particle velocity within the burnt mixture is caused by the fact that the gas adjacent to the wall expands by a factor of nearly six into the direction of the center. The magnitude of this velocity may be estimated from the observation that, when the flame surface is idealized to an impermeable wall that compresses the burnt mixture with a certain velocity, the ratio of the mass contained between the flame front and the surface where a fluid particle resides, and the mass contained between the latter and the vessel wall (see the upper-right part of Fig. 4) remains constant:

$$\frac{\frac{4}{3}\pi\rho_b[r_b^3(t)-r^3(t)]}{\frac{4}{3}\pi\rho_u[R_v^3-r_b^3(t)]+\frac{4}{3}\pi\rho_b[r_b^3(t)-r^3(t)]}=\text{constant}. \tag{12}$$

Differentiation with respect to time, and repeating the steps shown by Eqs. (3)–(6)

$$[(\rho_u/\rho_b)[R_v^3-r_b^3(t)]+[r_b^3(t)-r^3(t)]][r_b^3(t)-r^3(t)]' - [r_b^3(t)-r^3(t)][(\rho_u/\rho_b)[R_v^3-r_b^3(t)] + [r_b^3(t)-r^3(t)]]'=0 \tag{13}$$

$$\Leftrightarrow[(\rho_u/\rho_b)[R_v^3-r_b^3(t)]+[r_b^3(t)-r^3(t)]][3r_b^2(t)\dot{r}_b(t) - 3r^2(t)\dot{r}(t)]-[r_b^3(t)-r^3(t)][-3(\rho_u/\rho_b)r_b^2(t)\dot{r}_b(t) + 3r_b^2(t)\dot{r}_b(t)-3r^2(t)\dot{r}(t)]=0 \tag{14}$$

$$\Leftrightarrow R_v^3r^2(t)\dot{r}(t)-R_v^3r_b^2(t)\dot{r}_b(t)-r_b^3(t)r^2(t)\dot{r}(t) + r^3(t)r_b^2(t)\dot{r}_b(t)=0 \tag{15}$$

$$\Leftrightarrow r^2(t)[R_v^3-r_b^3(t)]\dot{r}(t)=r_b^2(t)[R_v^3-r^3(t)]\dot{r}_b(t), \tag{16}$$

again leads to Eq. (7). According to this result, the displacement velocity of a fluid particle increases progressively as the distance from the center becomes less, and would become infinitely large for a fluid particle residing at the center. The solution of Eq. (7) for the situation depicted by the upper-right part of Fig. 4, with $r_b(t)=33.0$ mm

and $\dot{r}_b(t) = -1.5$ m s^{-1} is shown in the lower part of Fig. 4. At a distance of 3 mm from the center, for example, the particle velocity is seen to increase to about 2000 m s^{-1}. With an assumed value of 0.1 kg m^{-3} for ρ_b, the expression for the dynamic pressure, $(1/2)\rho_b r^2(t)$ this velocity implies that pressure disturbances of about 2.0 bar are generated when the fluid particles lose their motion instantaneously. The reason for the smaller oscillations in the upper-left part of Fig. 3 must be sought in the fact that upon arrival at the sensor, the pressure waves are partly being absorbed and partly being reflected. It is the reflected part, which determines the magnitude of the experimentally observed pressure disturbances. Knowing that pressure disturbances scale quadratically with $\dot{r}_b(t)$, their absence at $\phi = 0.5$ in Fig. 2 may also be explained by Eq. (7). With the laminar burning velocity, and hence the flame speed, being three times smaller than in the case of stoichiometric mixtures, the pressure disturbances become nine times smaller, i.e. about 0.025 bar. This is close to the detection limit of the pressure sensor (0.2% of 10 bar).

4. Adapting the thin-flame model to the geometry of the 169 ml explosion vessel

A thin-flame model will now be derived for the explosion vessel shown in Fig. 1. This derivation is analogous to the one derived by Dahoe et al. (1996) and the resulting model is only valid while the radius of the flame is less than 20 mm (i.e. before the shape of the flame becomes distorted by interaction with the windows at a distance of 22 mm, or with the electrical insulation at a distance of 23 mm from the center). Following the derivation by Dahoe et al. (1996), the expression relating the rate of pressure rise to the mass burning rate (obtained from Eqs. (6) and (7) of Dahoe et al., 1996)

$$\frac{dP}{dt} = (P_{max} - P_0)\left(\frac{4\pi}{V_v}\right)\left(\frac{P}{P_0}\right)^{1/\gamma} r_f^2 S_{uL} \tag{17}$$

is combined with the expression that relates the flame radius to the instantaneous pressure (obtained from Eqs. (8) and (9) of Dahoe et al., 1996)

$$r_f = \left(\frac{3V_v}{4\pi}\right)^{1/3}\left[1 - \left(\frac{P_0}{P}\right)^{1/\gamma}\frac{P_{max} - P}{P_{max} - P_0}\right]^{1/3} \tag{18}$$

to give:

$$\frac{dP}{dt} = 3(P_{max} - P_0)\left(\frac{4\pi}{3V_v}\right)^{1/3}\left[1 - \left(\frac{P_0}{P}\right)^{1/\gamma}\frac{P_{max} - P}{P_{max} - P_0}\right]^{2/3} \times \left(\frac{P}{P_0}\right)^{1/\gamma} S_{uL}. \tag{19}$$

This expression, together with a correlation to incorporate the effect of changes in the pressure and temperature on the laminar burning velocity, as discussed in Section 5, will be fitted to the initial part of the experimental pressure–time curve. Note that Eqs. (17)–(19) are independent of the shape of the vessel, as long as there is no interaction between the flame and the wall. Moreover, as long as the radius of the flame does not exceed 20 mm, the problem may be idealized to a situation in which the flame propagates in a spherical vessel of the same volume.

5. The laminar burning velocity of hydrogen–air mixtures

The laminar burning velocity of hydrogen–air mixtures is known to depend on the chemical composition, the pressure, and the temperature. This sensitivity is commonly described by a power law expression of the form

$$\frac{S_{uL}}{S^o_{uL}} = \left(\frac{T_u}{T_{u0}}\right)^{\beta_1}\left(\frac{P}{P_0}\right)^{\beta_2}, \tag{20}$$

where S^o_{uL} denotes the laminar burning velocity at reference conditions of pressure and temperature, and S_{uL} the laminar burning velocity at arbitrary conditions of pressure and temperature. The dependence of S^o_{uL} on the equivalence ratio is shown in the upper part of Fig. 5. It is seen to assume a maximum value at an equivalence ratio of 1.6 and to decrease as the flammability limits are approached. The middle and lower part of Fig. 5 indicate that the laminar burning velocity of hydrogen–air mixtures increases with pressure and temperature. The linear dependence in the right part of these sub-figures implies that this behavior may be described by Eq. (20) and that the influence of temperature and pressure may be incorporated by the exponents β_1 and β_2. The latter are known to be a weak function of the equivalence ratio.

Iijima and Takeno (1986) observed that $\beta_1 = 1.54 + 0.026(\phi - 1)$ and $\beta_2 = 0.43 + 0.003(\phi - 1)$. These authors determined the value of β_1 and β_2 as a function of the equivalence ratio by assuming that

$$\frac{S_{uL}}{S^o_{uL}} = \left(\frac{T_u}{T_{u0}}\right)^{\beta_1}\left[1 + \beta_2 \ln\left(\frac{P}{P_0}\right)\right]. \tag{21}$$

Note that because this expression follows from Eq. (20) by the series expansion

$$a^{\beta_2} = 1 + \frac{\beta_2 \ln a}{1!} + \frac{(\beta_2 \ln a)^2}{2!} + \frac{(\beta_2 \ln a)^3}{3!} + \cdots + \frac{(\beta_2 \ln a)^n}{n!}, \tag{22}$$

β_2 in Eq. (20) will also exhibit a similar weak dependence. With this in mind, β_1 and β_2 were taken to be constant and equal to $(140.0 \pm 3.7) \times 10^{-2}$ and $(194.0 \pm 4.4) \times 10^{-3}$ in the present work. These values were determined from the experimental results reported by Iijima and Takeno (1986) on the influence of pressure and temperature on the laminar

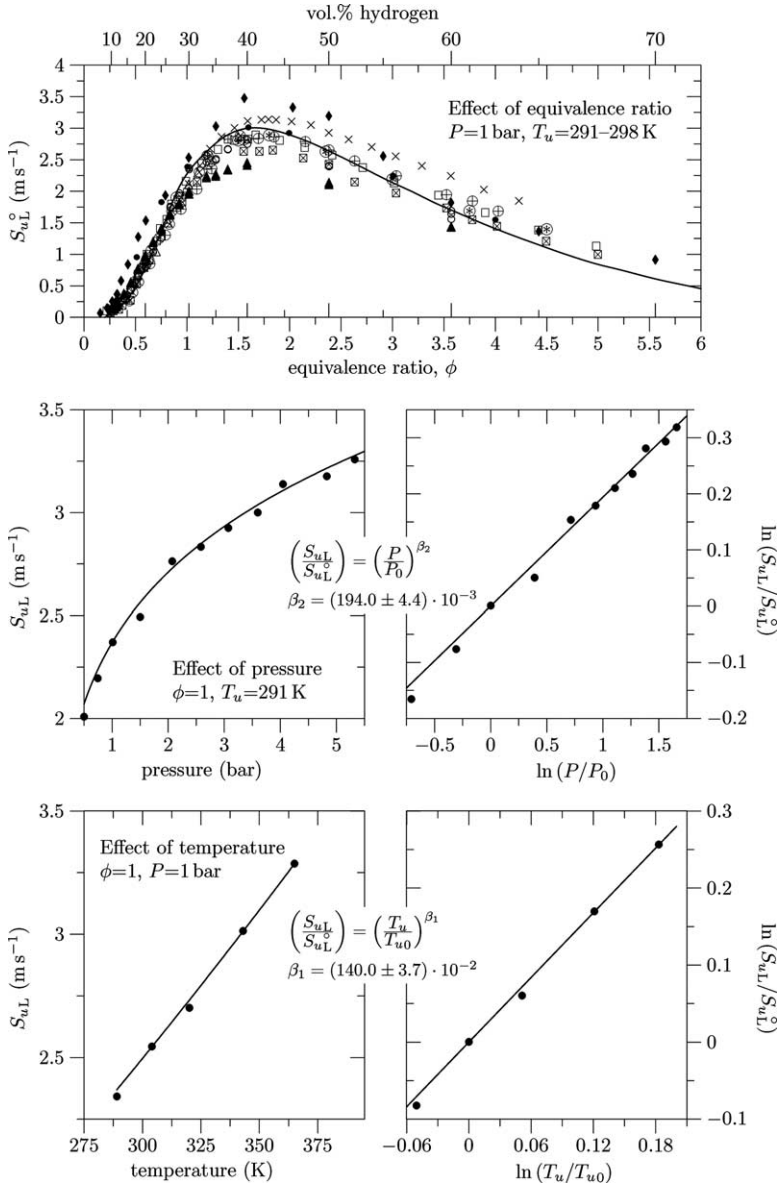

Fig. 5. Effect of equivalence ratio (upper part), pressure (middle-left part), and temperature (lower-left) on the laminar burning velocity of hydrogen–air mixtures (×: Takahashi, Mizomoto, & Ikai, 1983; □: Dowdy et al., 1990; ◆: Koroll, Kumar, & Bowles, 1993; ◇: Vagelopoulos, Egolfopoulos, & Law, 1995; •: Iijima & Takeno, 1986; ⊞: Wu & Law, 1984; △: Egolfopoulos & Law, 1990; ○: Lamoureux, Djebaili-Chaumeix, & Paillard, 2002, stretched; ▲: Lamoureux et al., 2002, unstretched; ⊛: Kwon & Faeth, 2001; ⊙: Law, 1993; ⊠: Aung et al., 1997; ⊕: Tse et al., 2000; solid line: Marinov et al., 1996).

burning velocity of hydrogen–air mixtures (see the middle and lower part of Fig. 5). Because of adiabatic compression of the unburnt mixture, the pressure and the temperature in Eq. (20) do not behave independently, but change simultaneously. This simultaneous change in pressure and temperature is taken into account by substituting the third expression of Eq. (1) into Eq. (20) so that

$$\frac{S_{uL}}{S_{uL}^{o}} = \left(\frac{P}{P_0}\right)^{\beta_2+\beta_1((\gamma-1)/\gamma)} = \left(\frac{P}{P_0}\right)^{\beta}. \tag{23}$$

With $\beta_1 = 1.4$, $\beta_2 = 0.194$, and $\gamma = 1.4$, it is seen that $\beta = 0.6$.

Eq. (23) was incorporated into Eq. (19) and the laminar burning velocity was determined by fitting the latter by means of the Levenberg–Marquardt method (Marquardt, 1963; Press et al., 1992) to the initial part of the pressure–time curves shown in Fig. 2 with S_{uL}^{o} as the only degree of freedom. This was accomplished by modifying the routine `mrqmin` by Press et al., such, that it enabled the fitting of a differential equation by its numerical solution to a set of discrete data points. The numerical solution of Eq. (19) was calculated by means of a fourth order Runge–Kutta method, using the routine `rkdumb` by the same authors. Owing to the lower experimental maximum explosion pressures due to the size of the vessel, as discussed in Section 2,

and the uncertainty introduced by the oscillations in the experimental pressure–time curve, the theoretical values shown in the middle of Fig. 2 have been used for P_{max} in Eq. (19). To minimize modification of the laminar burning velocity by flame curvature and flame acceleration due to excessive spark ignition energies in the initial stage of the explosions, and to avoid flame–wall interaction, Eq. (19) was fitted to the early part of the pressure–time curves where the pressure changed from 1.15 to 1.3 bar. It may be verified by means of Eq. (18) that with all equivalence ratios, the flame radius varies between 15 and 20 mm when the pressure changes between 1.15 and 1.3 bar. This is indicated by the shaded region in the left part of Fig. 1. The correspondence between the solution of Eq. (19) and the experimental data is illustrated by the middle-left and lower-left part of Fig. 6.

The upper part of Fig. 6 shows a comparison between the optimal values of the laminar burning velocity, S^{o}_{uL}, obtained by fitting Eq. (19), and values reported by other researchers. The shaded region in the upper-left part denotes the band of data shown in Fig. 5. It is seen that the laminar burning velocities obtained in this work fall within the band of data reported by other researchers. The upper-right part shows a comparison with laminar burning velocities computed by Marinov, Westbrook, and Pitz (1996) by means of a detailed kinetic scheme, and experimental data that was obtained by more advanced methods (Dowdy et al., 1990; Kwon & Faeth, 2001; Tse et al., 2000). This comparison indicates that laminar burning velocities at equivalence ratios greater than 0.75, obtained by fitting an integral balance model to the pressure curve fall within the scatter of those produced by more advanced methods. Therefore, more advanced methods that take stretch effects into account have little or no advantage over the traditional method. This conclusion is in agreement with an earlier observation involving the data by Iijima and Takeno (1986),

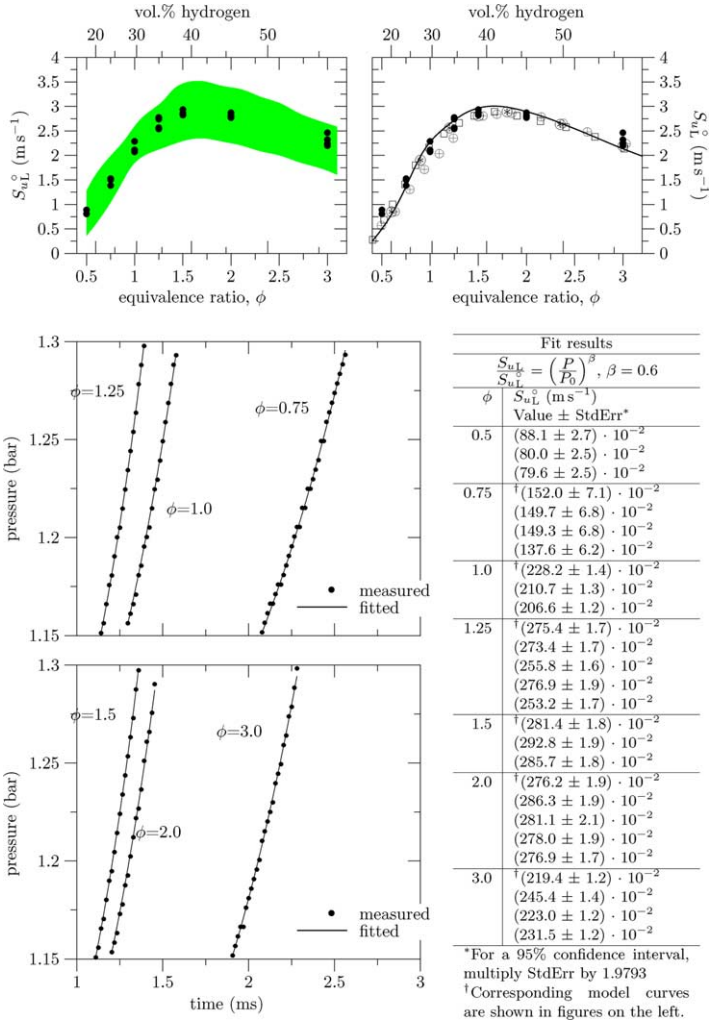

Fit results

$\frac{S_{uL}}{S_{uL}^{\circ}} = \left(\frac{P}{P_0}\right)^{\beta}$, $\beta = 0.6$

ϕ	S°_{uL} (m s^{-1}) Value ± StdErr*
0.5	$(88.1 \pm 2.7) \cdot 10^{-2}$
	$(80.0 \pm 2.5) \cdot 10^{-2}$
	$(79.6 \pm 2.5) \cdot 10^{-2}$
0.75	†$(152.0 \pm 7.1) \cdot 10^{-2}$
	$(149.7 \pm 6.8) \cdot 10^{-2}$
	$(149.3 \pm 6.8) \cdot 10^{-2}$
	$(137.6 \pm 6.2) \cdot 10^{-2}$
1.0	†$(228.2 \pm 1.4) \cdot 10^{-2}$
	$(210.7 \pm 1.3) \cdot 10^{-2}$
	$(206.6 \pm 1.2) \cdot 10^{-2}$
1.25	†$(275.4 \pm 1.7) \cdot 10^{-2}$
	$(273.4 \pm 1.7) \cdot 10^{-2}$
	$(255.8 \pm 1.6) \cdot 10^{-2}$
	$(276.9 \pm 1.9) \cdot 10^{-2}$
	$(253.2 \pm 1.7) \cdot 10^{-2}$
1.5	†$(281.4 \pm 1.8) \cdot 10^{-2}$
	$(292.8 \pm 1.9) \cdot 10^{-2}$
	$(285.7 \pm 1.8) \cdot 10^{-2}$
2.0	†$(276.2 \pm 1.9) \cdot 10^{-2}$
	$(286.3 \pm 1.9) \cdot 10^{-2}$
	$(281.1 \pm 2.1) \cdot 10^{-2}$
	$(278.0 \pm 1.9) \cdot 10^{-2}$
	$(276.9 \pm 1.7) \cdot 10^{-2}$
3.0	†$(219.4 \pm 1.2) \cdot 10^{-2}$
	$(245.4 \pm 1.4) \cdot 10^{-2}$
	$(223.0 \pm 1.2) \cdot 10^{-2}$
	$(231.5 \pm 1.2) \cdot 10^{-2}$

*For a 95% confidence interval, multiply StdErr by 1.9793
†Corresponding model curves are shown in figures on the left.

Fig. 6. Upper part: a comparison between laminar burning velocities obtained by fitting the thin-flame model to experimental pressure–time curves and values reported by other researchers (shaded region: data band shown in the upper part of Fig. 5; solid line: computed data by Marinov et al., 1996; □: Dowdy et al., 1990; ⊛: Kwon & Faeth, 2001; ⊕: Tse et al., 2000; •: this work). Middle-left and lower-left part: comparison between the model curves and measured data.

as discussed in Section 1. The laminar burning velocity at an equivalence ratio of 0.5 is larger than the stretch-corrected ones, but still close enough to the latter to be suitable as a conservative input for the assessment of accidental combustion hazards.

The absence of a significant advantage by more advanced methods that take flame stretch into account over the traditional method employed in the present work with fuel-rich mixtures, and the consistently higher laminar burning velocities produced by the latter with fuel-lean mixtures, deserve some further clarification. It has been observed experimentally that flames develop into wrinkled structures when the limiting reactant in a combustible mixture is also the more mobile constituent. This phenomenon is known to begin with flame cracking, followed by a further development into a cellular structure (Bradley, 1999; Bradley, Cresswell, & Puttock, 2001; Bradley & Harper, 1994; Bradley, Hicks, Lawes, Sheppard, & Woolley, 1998; Bradley, Sheppard, Woolley, Greenhalgh, & Lockett, 2000; Groff, 1982; Gu, Haq, Lawes, & Woolley, 2000; Haq, Sheppard, Woolley, Greenhalgh, & Lockett, 2002). The role of the limiting reactant in cell formation is clearly demonstrated by the work of Tse et al. (2000). These authors presented Schlieren photographs of spark ignited spherically propagating flames in $H_2/O_2/N_2$- and H_2/O_2/He-mixtures, at initial conditions of 298 K and 3, 5, 20, 40, and 60 atm. Some of these photographs are included in the upper part of Fig. 7 to support the present discussion. Pictures of $H_2/O_2/N_2$-flames at equivalence ratios of 0.70 and 2.25 (ignited at 3 and 5 atm), 0.85 and 1.50 (ignited at 20 atm), and 3.5 (ignited at 40 and 60 atm), and of H_2/O_2/He-flames, at equivalence ratios of 0.70 and 2.25 (ignited at 3 and 5 atm), 0.85 and 1.50 (ignited at 20 atm), and 0.70 (ignited at 40 and 60 atm), were presented. With $H_2/O_2/N_2$-flames, it may be observed that, when the equivalence ratio is less than unity, and hence the more mobile constituent becomes the limiting reactant, the flame surface is initially distorted by large-scale wrinkles that originate from system perturbations, and subsequently by wrinkles of an ever decreasing size, down to a magnitude in the order of the laminar flame thickness (see the lower-right part of Fig. 7). When the equivalence ratio is greater than unity, $H_2/O_2/N_2$-flames appear to be free of wrinkles at low pressure (e.g. at 3 atm), and contain only large-scale wrinkles arising from system perturbations at higher pressures (e.g. 5, 20, 40, and 60 atm). No cascade of wrinkles from large to small-scale appears to be present during the growth of the flame. With H_2/O_2/He-flames (i.e. with N_2 being replaced by He, the limiting reactant can no longer be the more mobile one), this cascade of wrinkles turns out to be absent for all equivalence ratios and only large-scale wrinkles are seen to evolve at higher pressures (e.g. 20, 40, and 60 atm).

The development of a flame surface into a wrinkled structure causes the true laminar burning velocity, S_{uL}, to deviate from the unstretched laminar burning velocity, S^*_{uL}, i.e. the magnitude it would have if the flame were planar. This modification is caused by two distinct, but invariably coupled effects, namely, the effect of flame curvature (see the middle-right part of Fig. 7) and the effect of flame stretch (see the lower-left part of Fig. 7). When a flame is bulged into concavity with respect to the unburnt mixture, heat which is initially conducted into the unburnt mixture, is subsequently convected to parts of the flame closer to the center. This process enhances the laminar burning velocity at the center and reduces the laminar burning velocity at the lateral parts of the flame. When the flame is convex with respect to the unburnt mixture, the opposite happens: heat is conducted into the unburnt mixture and convected away from the center. This reduces the laminar burning velocity at the center and increases the laminar burning velocity of the lateral parts. The presence of a wrinkled flame causes the flow-field of the approaching unburnt mixture to become non-uniform. Because of the non-zero velocity gradients in the unburnt mixture, fluid elements approaching a wrinkled flame are no longer the same as those approaching a planar flame. As illustrated by lower-left part of Fig. 5, fluid elements, respectively, undergo compression or stretch, prior to being consumed by a concave or convex flame surface. The compression of fluid elements enhances the laminar burning velocity due to the increase in the mass flow of reactants entering the flame per unit area. The stretching of fluid elements reduces the mass flow of reactants into the flame, and hence the laminar burning velocity. To cope with this situation, various researchers have attempted to establish relationships between the true laminar burning velocity of a wrinkled flame and the unstretched laminar burning velocity. To support the present discussion, Eq. (13) by Dahoe, Hanjalic, and Scarlett (2002) is quoted here as an example:

$$S_{uL} = \mathcal{L}_s[\boldsymbol{nn} : \nabla \boldsymbol{v} - \nabla \cdot \boldsymbol{v}] + [1 - \mathcal{L}_c \nabla \cdot \boldsymbol{n}] S^*_{uL}$$

$$= \mathcal{L}_s[\boldsymbol{nn} : \nabla \boldsymbol{v} - \nabla \bullet \boldsymbol{v}] + \left[1 + \frac{\mathcal{L}_c}{\mathcal{R}}\right] S^*_{uL} \qquad (24)$$

The reader may consult Dahoe et al. (2002) and references cited therein for further information on its origin and motivation. In this equation, $\boldsymbol{nn}$: $\nabla \boldsymbol{v} - \nabla \cdot \boldsymbol{v}$ denotes the stretch intensity, $\mathcal{R}$ the local radius of curvature, $\mathcal{L}_s$ the stretch Markstein length and $\mathcal{L}_c$ the curvature Markstein length. The latter are proportionality constants between the laminar burning velocity and effects due to stretch and curvature.

Eq. (24) may be used to compare the laminar burning velocities obtained by the traditional method, with those obtained by more advanced methods shown in the upper-right part of Fig. 6. When $\phi \geq 1.0$, the more mobile constituent of the mixture is no longer the limiting reactant, and the flame surface remains smooth. With stretch effects due to velocity gradients being small, and the radius of curvature (i.e. 15 mm $\leq \mathcal{R} \leq$ 20 mm) being much larger than the curvature Markstein length (this is known to be in

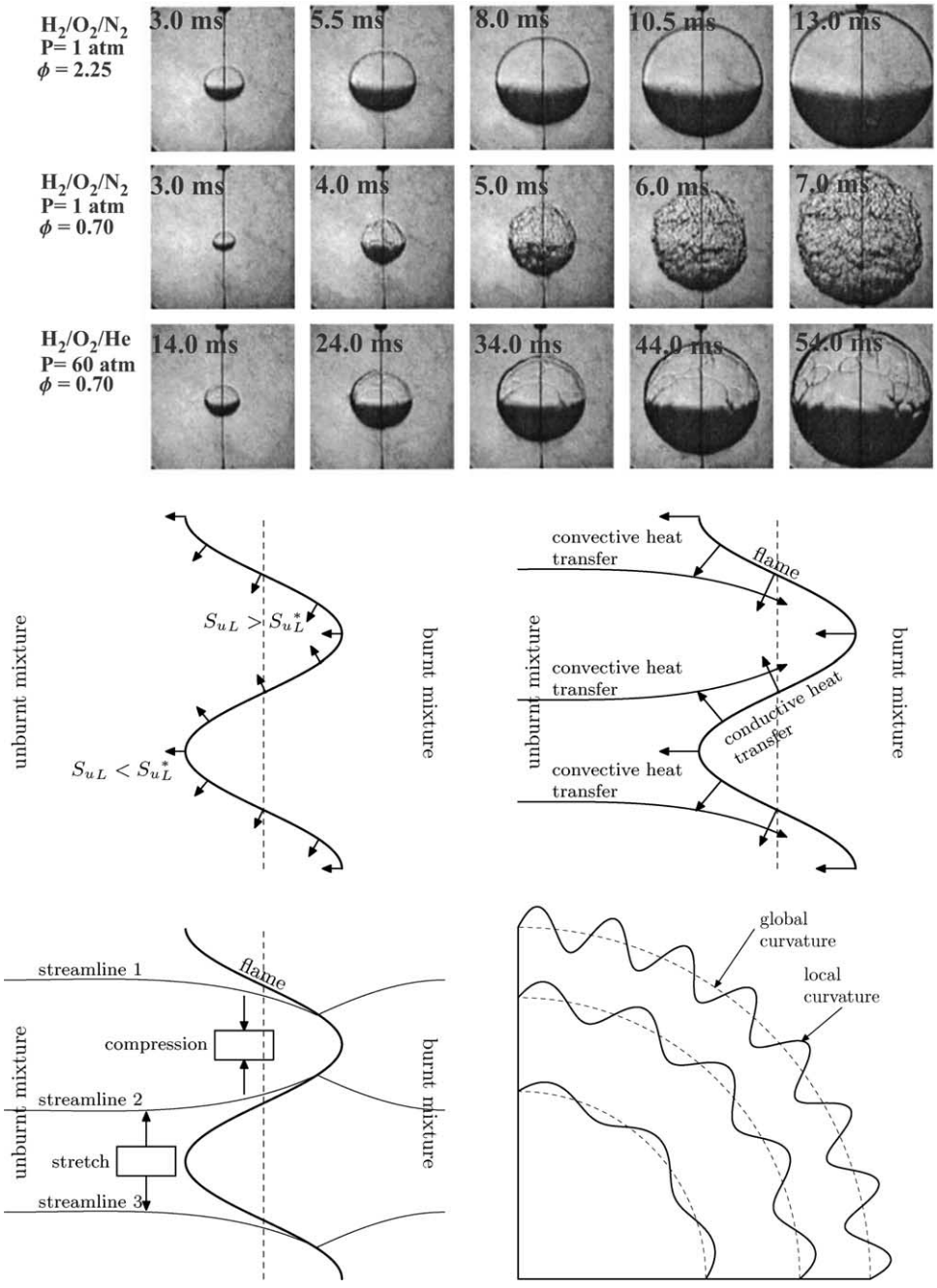

Fig. 7. Upper part: pictures by Tse et al. (2000) showing the development of small-scale wrinkles when the limiting reactant is also the more mobile constituent of a combustible mixture. Middle-left part: modification of the laminar burning velocity by the development of flame curvature. Middle-right part: the role of heat conduction and convective heat transfer in the modification of the laminar burning velocity of curved flames. Lower-left part: the role of flame stretch in the modification of the laminar burning velocity. Lower-right part: the cascading of large-scale wrinkles to small-scale wrinkles during flame growth.

the order of the laminar flame thickness which is less than 0.5 mm for hydrogen–air mixtures), it becomes obvious that the performance of the more advanced methods will not differ significantly from the method applied in the present work. This situation becomes different when $\phi < 1.0$. As discussed previously, laminar flames develop into wrinkled flames when the limiting reactant is also the more mobile constituent. The photographs by Tse et al. (2000) in the upper part of Fig. 7 (the frame diagonal is 74 mm) show that an initially smooth hydrogen–air flame at $\phi = 0.7$ contains only large-scale wrinkles when its radius has grown to 8 mm at 4 ms, the cascade process to small-scale wrinkles is well underway at 5 ms when the radius is 11.5 mm, and that this cascade process has reached an equilibrium when the flame radius has become 17 mm at 6 ms. With this in mind, the agreement between the laminar burning velocity at $\phi = 0.75$ obtained by the methodology applied in the present work and that from more advanced methods may be explained by

arguing that the flame surface does not contain sufficient small-scale wrinkles when the flame radius is between 15 and 20 mm. It is emphasized, however, that photographs of the flame morphology at $\phi = 0.75$ are needed to verify this argument. Following the same reasoning, the higher laminar burning velocity at $\phi = 0.5$ is easily explained. Based on the observations by Tse et al. (2000), it is obvious that the flame surface at $\phi = 0.5$ consists of small-scale wrinkles when the flame radius is between 15 and 20 mm. In this situation, the application of Eq. (19) boils down to evaluating the product of a wrinkled flame surface and the true laminar burning velocity as the product of a smooth spherical flame surface area coinciding with the global flame curvature (see the lower-right part of Fig. 7) and a surface averaged laminar burning velocity. While a surface averaged laminar burning velocity would make sense because crests in the flame surface are compensated by troughs, this idealization does not take the increase in flame surface area due to flame wrinkling into account. This deficiency leads to a higher laminar burning velocity.

6. Conclusions

Laminar burning velocities of hydrogen–air mixtures were determined from closed vessel gas explosions. Initially quiescent mixtures were ignited in a 169 ml vessel, the pressure was measured as a function of time, and an integral balance model (i.e. Eq. (19)) was fitted to the experimental pressure–time curve to extract the laminar burning velocity. The equivalence ratio varied from 0.5 to 3.0, and all experiments were conducted at initial conditions of 1 bar and 293 K. Inaccuracies due to the flame curvature and flame acceleration caused by excessive spark ignition energies in the initial stage of the explosions, as well as those arising from flame–wall interaction, were avoided by using only the part of the pressure–time curves between 1.15 and 1.3 bar (see the middle-left and lower-left part of Fig. 6). A correlation for the effect of pressure and temperature on the laminar burning velocity (i.e. Eq. (20)) was incorporated into the integral balance model to avoid further inaccuracies caused by changes in the thermodynamic of the unburnt mixture in the course of the explosions. The resulting laminar burning velocities were subsequently compared with those reported in the literature. The conclusions arising from this comparison are as follows:

- Laminar burning velocities of fuel-rich mixtures obtained by the methodology followed in the present paper are seen to fall within the scatter of data obtained by more advanced methods that take the influence of flame stretch into account (see the upper-right part of Fig. 6. This observation implies that, with fuel-rich mixtures, more advanced methods have no significant advantage over methodologies that rely only on pressure variations from windowless explosion vessels for the determination of the laminar burning velocity. Moreover, with fuel-rich mixtures, the cost-benefit balance is in favor of the latter.
- Laminar burning velocities of fuel-lean mixtures are seen to be consistently higher, but at the same time close enough to the ones obtained by more advanced methods. Because of this, they may be considered as acceptable conservative estimates of the laminar burning velocity for engineering calculations that form the design basis for fire and explosion safety.

The pressure–time curves of hydrogen–air mixtures are seen to exhibit pressure oscillations (see Fig. 2), which are absent when methane–air mixtures for example (see Fig. 6 by Dahoe & de Goey, 2003), are ignited to deflagration at the same initial conditions. These oscillations were considered in Section 3, and an Eq. (7) was derived to describe their cause. The implications of this equation are that combusting fluid layers adjacent to the wall are inducing particle velocities in the order of kilometers per second which in turn give rise to pressure spikes. The magnitude of these particle velocities is directly proportional to the flame speed, quadratically proportional to $r_b(t)$ the vessel radius, and inversely proportional to the distance from the wall where flow reversal occurs $R_n^3(t) - r_b^3(t)$. Of these three proportionalities, the last one is the subject of most concern. For combustible mixtures such as hydrogen–air and hydrogen–oxygen mixtures, this last proportionality may give rise to high-pressure spikes because of the small flame thickness. It is easy to see that the distance from the vessel wall where flow reversal occurs, and hence $R_n^3(t) - r_b^3(t)$, decreases when the flame thickness becomes smaller. As a result, the handling of such mixtures involves an additional safety problem which is absent with hydrocarbon–air mixtures. This may impose a limitation on the use of hydrogen as an energy carrier with at least the same level of safety and comfort as with today's fossil fuel energy carriers.

Acknowledgements

The experiments described in this paper were conducted by a group of undergraduate students at the Department of Mechanical Engineering of Eindhoven University of Technology, namely, Bram van Benthum, Jean-Pierre Thoolen, Harrie Smetsers and Joris Wismans. The contribution and the support of Philip de Goey to this work are gratefully acknowledged.

References

Agnew, J. T., & Graiff, L. B. (1961). The pressure dependence of laminar burning velocity by the spherical bomb method. *Combustion and Flame*, *5*, 209–219.

Aung, K. T., Hassan, M. I., & Faeth, G. M. (1997). Flame stretch interactions of laminar premixed hydrogen/air flames at normal temperature and pressure. *Combustion and Flame*, *109*, 1–24.

Aung, K. T., Hassan, M. I., & Faeth, G. M. (1998). Effects of pressure and nitrogen dilution on flame/stretch interactions of laminar premixed $H_2/O_2/N_2$ flames. *Combustion and Flame*, *112*, 1–15.

Babkin, V. S., Bukharov, V. N., & Molkov, V. V. (1989). Normal flame velocity of propane–air mixtures at high pressures and temperatures. *Fizaka Goreniya i Vzryva*, *25*, 57–63 (English translation in Combustion, Explosion and Shock Waves).

Babkin, V. S., Vyun, A. V., & Kozachenko, L. S. (1967). The determination of burning velocity in a constant volume bomb by pressure recording. *Fizaka Goreniya i Vzryva*, *3*, 362–370 (English translation in Combustion, Explosion and Shock Waves).

Bradley, D. (1999). Instabilities and flame speeds in large-scale premixed gaseous explosions. *Philosophical Transactions of the Royal Society of London, Series A*, *357*, 3567–3581.

Bradley, D., Cresswell, T. M., & Puttock, J. S. (2001). Flame acceleration due to flame-induced instabilities in large-scale explosions. *Combustion and Flame*, *124*, 551–559.

Bradley, D., & Harper, C. M. (1994). The development of instabilities in laminar explosion flames. *Combustion and Flame*, *99*, 562–572.

Bradley, D., Hicks, R. A., Lawes, M., Sheppard, C. G. W., & Woolley, R. (1998). The measurement of laminar burning velocities and Markstein numbers for iso-octane air and iso-octanen–heptane air mixtures at elevated temperatures and pressures in an explosion bomb. *Combustion and Flame*, *115*, 126–144.

Bradley, D., Sheppard, C. G. W., Woolley, R., Greenhalgh, D. A., & Lockett, R. D. (2000). The development and structure of flame instabilities and cellularity at low Markstein numbers in explosions. *Combustion and Flame*, *122*, 195–209.

Brown, M. J., McLean, I. C., Smith, D. B., & Taylor, S. C. (1996). Markstein lengths of CO/H_2/air flames using expanding spherical flames. *Twenty-sixth symposium (international) on combustion.* (pp. 875–881). Pittsburgh, PA: The Combustion Institute.

Cashdollar, K. L., Zlochower, I. A., Green, G. M., Thomas, R. A., & Hertzberg, M. (2000). Flammability of methane, propane, and hydrogen gases. *Journal of Loss Prevention in the Process Industries*, *13*, 327–340.

Clarke, A., Stone, R., & Beckwith, P. (2001). Measurement of the laminar burning velocity of *n*-butane and isobutane mixtures under micro-gravity conditions in a constant volume vessel. *Journal of the Institute of Energy*, *74*, 70–76.

Dahoe, A. E., & de Goey, L. P. H. (2003). On the determination of the laminar burning velocity from closed vessel gas explosions. *Journal of Loss Prevention in the Process Industries*, *16*, 457–478.

Dahoe, A. E., Hanjalic, K., & Scarlett, B. (2002). Determination of the laminar burning velocity and the Markstein length of powder-air flames. *Powder Technology*, *22*, 222–238.

Dahoe, A. E., Zevenbergen, J. F., Lemkowitz, S. M., & Scarlett, B. (1996). Dust explosions in spherical vessels: The role of flame thickness in the validity of the 'cube-root-law'. *Journal of Loss Prevention in the Process Industries*, *9*, 33–44.

Dowdy, D. R., Smith, D. B., Taylor, S. C., & Williams, A. (1990). The use of expanding spherical flames to determine burning velocities and stretch effects in hydrogen–air mixtures. *Twenty-third symposium (international) on combustion.* (pp. 325–332). Pittsburgh, PA: The Combustion Institute.

Egolfopoulos, F. N., & Law, C. K. (1990). An experimental and computational study of the burning rates of ultra-lean to moderately rich $H_2/O_2/N_2$ laminar flames with pressure variations. *Twenty-third symposium (international) on combustion.* (pp. 333–346). Pittsburgh, PA: The Combustion Institute.

Garforth, A. M., & Rallis, C. J. (1976). Gas movement during flame propagation in a constant volume bomb. *Acta Astronautica*, *3*, 879–888.

Groff, E. G. (1982). The cellular nature of confined spherical propane–air flames. *Combustion and Flame*, *48*, 51–62.

Gu, X. J., Haq, M. Z., Lawes, M., & Woolley, R. (2000). Laminar burning velocities and Markstein lengths of methane–air mixtures. *Combustion and Flame*, *121*, 41–58.

Halstead, M. P., Pye, D. B., & Quinn, C. P. (1974). Laminar burning velocities and weak flammability limits under engine-like conditions. *Combustion and Flame*, *22*, 89–97.

Haq, M. Z., Sheppard, C. G. W., Woolley, R., Greenhalgh, D. A., & Lockett, R. D. (2002). Wrinkling and curvature of laminar and turbulent premixed flames. *Combustion and Flame*, *131*, 1–15.

Hassan, M. I., Aung, K. T., & Faeth, G. M. (1997). Properties of laminar premixed CO/H_2/air flames at various pressures. *Journal of Propulsion and Power*, *13*, 239–245.

Hassan, M. I., Aung, K. T., & Faeth, G. M. (1998). Measured and predicted properties of laminar premixed methane/air flames at various pressures. *Combustion and Flame*, *115*, 539–550.

Iijima, T., & Takeno, T. (1986). Effects of temperature and pressure on burning velocity. *Combustion and Flame*, *12*, 445–452.

Koroll, G. W., Kumar, R. K., & Bowles, E. M. (1993). Burning velocities of hydrogen–air mixtures. *Combustion and Flame*, *94*, 330–340.

Kwon, O. C., & Faeth, G. M. (2001). Flame/stretch interactions of premixed hydrogen-fueled flames: Measurements and predictions. *Combustion and Flame*, *124*, 590–610.

Kwon, O. C., Tseng, L.-K., & Faeth, G. M. (1992). Laminar burning velocities and transition to unstable flames in $H_2/O_2/N_2$ and $C_2H_8/O_2/N_2$ mixtures. *Combustion and Flame*, *90*, 230–246.

Lamoureux, N., Djebaili-Chaumeix, N., & Paillard, C. E. (2002). Laminar flame velocity determination for H2–air–steam mixtures using the spherical bomb method. *Journal de Physique de France IV*, *12*, 445–452.

Law, C. K. (1993). A compilation of experimental data on laminar burning velocities. In N. Peters, & B. Rogg (Eds.), *Reduced kinetic mechanisms for applications in combustion systems* (pp. 15–26). Berlin: Springer, 15–26.

Law, C. K., Zhu, D. L., & Yu, G. (1988). Propagation and extinction of stretched premixed flames. *Proceedings of the 21st symposium (international) on combustion.* (pp. 1419–1426). Pittsburgh, PA: The Combustion Institute.

Lewis, B., & von Elbe, G. (1961). *Combustion, flames and explosions of gases* (2nd ed). New York: Academic Press.

Marinov, N. M., Westbrook, C. K., & Pitz, W. J. (1996). Detailed and global chemical kinetics model for hydrogen. In S. H. Chan, *Transport phenomena in combustion* (Vol. 1) (pp. 118–129). Washington, DC: Taylor & Francis.

Marquardt, D.W. (1963). An algorithm for least squares estimation of nonlinear parameters. *SIAM Journal on Applied Mathematics, 11*, 431–441.

Metghalchi, M., & Keck, J. C. (1980). Laminar burning velocity of propane–air mixtures at high temperature and pressure. *Combustion and Flame*, *38*, 143–154.

Metghalchi, M., & Keck, J. C. (1982). Burning velocities of mixtures of air with methanol, isooctane, and indolene at high pressure and temperature. *Combustion and Flame*, *48*, 191–210.

Milton, B. E., & Keck, J. C. (1984). Laminar burning velocities in stoichiometric hydrogen and hydrogen–hydrocarbon gas mixtures. *Combustion and Flame*, *58*, 13–22.

Molkov, V. V., & Nekrasov, V. P. (1981). Normal propagation velocity of acetone–air flames versus pressure and temperature. *Fizaka Goreniya i Vzryva*, *17*, 45–49 (English translation in Combustion, Explosion and Shock Waves).

Press, W. H., Teukolsky, S. A., Vetterling, W. T., & Flannery, B. P. (1992). *Numerical recipes in PASCAL. The art of scientific computing* (2nd ed.). Cambridge: Cambridge University Press.

Rallis, J. C., Garforth, A. M., & Steinz, J. A. (1965). Laminar burning velocity of acetylene–air mixtures by the constant-volume method. *Combustion and Flame*, *9*, 345–356.

Savitzky, A., & Golay, M. J. E. (1964). Smoothing and differentiation of data by simplified least squares procedures. *Analytical Chemistry*, *36*, 1627–1639.

Takahashi, F., Mizomoto, M., & Ikai, S. (1983). Alternative energy sources III. In T. Nejat Veziroglu, *Nuclear energy/synthetic fuels* (Vol. 5) (pp. 447–457). New York: McGraw-Hill.

Tse, S. D., Zhu, D. L., & Law, C. K. (2000). Morphology and burning rates of expanding spherical flames in H_2/O_2/inert mixtures up to 60 atmospheres. *Proceedings of the 28th symposium (international) on combustion.* (pp. 1793–1800). Pittsburgh, PA: The Combustion Institute.

Tseng, L.-K., Ismail, M. A., & Faeth, G. M. (1993). Laminar burning velocities and Markstein numbers of hydrocarbon/air flames. *Combustion and Flame*, *95*, 410–426.

Vagelopoulos, C. M., Egolfopoulos, F. N., & Law, C. K. (1995). Further considerations on the determination of laminar flame speeds from stretched flames. *Proceedings of the 25th symposium (international) on combustion.* (pp. 1341–1347). Pittsburgh, PA: The Combustion Institute.

Wu, C. K., & Law, C. K. (1984). On the determination of laminar flame speeds from stretched flames. *Proceedings of the 20th symposium (international) on combustion.* (pp. 1941–1949). Pittsburgh, PA: The Combustion Institute.

Yu, G., Law, C. K., & Wu, C. K. (1986). Laminar flame speeds of hydrocarbon + air mixtures with hydrogen addition. *Combustion and Flame*, *63*, 339–347.

Zhu, D. L., Egolfopoulos, F. N., & Law, C. K. (1989). Experimental and numerical determination of laminar flame speeds of methane/(Ar, N_2, CO_2)–air mixtures as function of stoichiometry, pressure, and flame temperature. *Proceedings of the 22nd symposium (international) on combustion.* (pp. 1537–1545). Pittsburgh, PA: The Combustion Institute.